

A Fluid-Actuated Driving Mechanism for Rolling Robots

Seyed Amir Tafrishi¹, Esmaeil Esmaeilzadeh² Mikhail Svinin³ and Motoji Yamamoto¹

Abstract—There are important issues in the design of the driving mechanism for the rolling robots. The actuator is expected to operate without occupying the whole space of the carrier body. This property gets harder to achieve as the degree of freedom in driving mechanism increases. This paper proposes an alternative fluid actuator for rolling bodies e.g., sphere or disc. The designed mechanism has a circular pipe that is propelled by rotating spherical mass (core) inside a fluid medium. In this work, we first establish the dynamics of the rolling circular pipe. Then, the internal driving unit is modeled and combined with rotating mass dynamics. Finally, the model simulations are conducted for observing motion patterns of the carrier body and locomotion abilities of the rotating core. The results show the feasibility of the proposed actuator for future applications.

I. INTRODUCTION

Rolling robots are increasingly being involved in unmanned ground vehicle researches. Li and Canny were the first scholars who studied the controllability of rolling objects as a non-holonomic system [1]. Since then, many types of research have taken place to develop a rolling robot for real-world applications [2]. However, there are certain challenges in the design of these robots that cannot be satisfied, e.g., having an isolated driver, omni-directional locomotion of the robot.

In the literature on spherical rolling robots, different principles of actuation have been studied. First, spherical robots were developed based on the torque-reaction principle [3]–[6]. To move these robots, mounted internal wheels were creating the reaction force opposed to the spherical shell. Another principle of propulsion was changing the center of mass inside the spherical body [7], [8] where certain weights were moving through a connecting rod. As an alternative in mass-imbalance mechanism, pendulum-based robots were also proposed [9], [10]. Different scholars studied trajectory tracking methods for this model [11]–[13] because this type could combine torque-reaction and mass-imbalance to propel itself. Also, some robots were conserving their angular momentum through rotating discs to carry their body [14]–[16]. Gyrover was an example for the disk-like robot with a rotating internal gyroscope and two motor drivers [14]. Another hybrid spherical robot was implemented with combining conservation of angular momentum and torque-reaction forces at MIT [17].

It should be noted that there are certain downsides in the previously proposed actuators. For example, a pendulum-

actuated system has an efficient mechanism and realizable dynamics [18]. However, increasing the number of pendulums for multiple degrees of freedom is not feasible due to the collision of connecting rods. Typically, most mechanisms occupy the whole space of spherical shell [2]. This issue prevents including any extra equipment to the robot. To deal with complete occupancy of the inner body, moving masses attached to the geared bars are the only solution [7], [8]. Nevertheless, gears directly limit the velocity of these mass-imbalance actuators because there are load inertia and motor backlash [7]–[9], [17], [19]. To address these problems, we propose a fluid actuated mechanism. To manipulate a carrier body, the fluid pushes a spherical moving mass (core) within a circular pipe. This removes the limitation of gear-based equipment and makes the core motion directly dependent on the injected fluid properties. Additionally, combining these mechanisms increases the degree of mobility in the rolling carrier/robot. In the proposed mechanism, the fluid is moved by a cylinder that is connected to a linear actuator. By moving the rod inside the linear actuator and the cylinder, the injected fluid volume is controlled. Note that fluid circulation guarantees a safe and smooth work of the propulsion mechanism during locomotion.

In this paper, we focus on modeling the novel driving mechanism and combine it with the dynamics of the rolling pipe. We simulate this mechanism for two case studies: motion patterns of rolling body and locomotion ability of the core. These simulations are necessary for estimating the power of this actuator. This mechanism will be applied to develop the proposed robot in [20].

We organize the paper as follows. The dynamics of the rolling body are derived by the Lagrange-Euler method in Section II. In Section III, the internal driving mechanism is described and modeled. Next, the rolling body and the driving unit are combined in Section IV. Finally, Section V analyzes the simulation results of the proposed actuator.

II. ROLLING BODY DYNAMICS

To derive the dynamics of the rolling body, variables and coordinate frames are considered as Fig. 1. Here, $X_0Y_0Z_0$ represents the inertial reference frame. The moving frame connected to the center of the circular pipe is $X_1Y_1Z_1$, which translates with respect to inertial frame $X_0Y_0Z_0$. Also, $X_2Y_2Z_2$ is a rotating frame for the core attached to the center of the pipe, but it rotates with respect to the $X_1Y_1Z_1$.

Moving mass (core) is traveling through the dashed line as shown in Fig. 1-a. The kinematic model of the spherical carrier (linear and angular velocities are \mathbf{V}_b and $\boldsymbol{\omega}_b$) and the core as a moving point (linear and angular velocities are \mathbf{V}_c

¹ Seyed Amir Tafrishi and Motoji Yamamoto are with the Department of Mechanical Engineering, Kyushu University, Kyushu, Japan amir@ce.mech.kyushu-u.ac.jp and yama@mech.kyushu-u.ac.jp

² Esmaeil Esmaeilzadeh is with the Department of Mechanical Engineering, University of Tabriz, Tabriz, Iran esmzadeh@tabrizu.ac.ir

³ Mikhail Svinin is with the Department of Information Science and Engineering, Ritsumeikan University, Kyoto, Japan svinin@fc.ritsumei.ac.jp

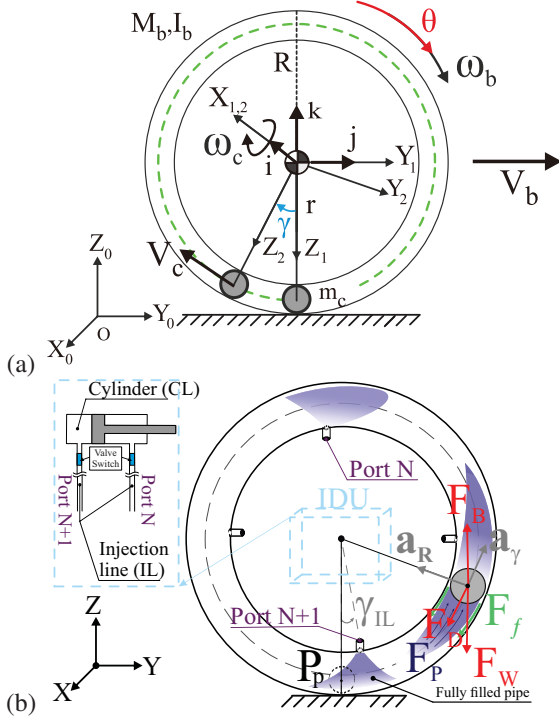


Fig. 1: a) Rolling motion model along $O - Y$ with core in circular pipe, b) Forces on the core due to the fluid circulation. Note: \mathbf{F}_B , \mathbf{F}_D , \mathbf{F}_W , \mathbf{F}_f and \mathbf{F}_P are buoyancy, drag, weight, surface friction and dynamic pressure forces, respectively.

and ω_c) in 2D plane is

$$\begin{aligned} \mathbf{D}_{co} &= -r \sin(\gamma + \theta) \mathbf{j} - r \cos(\gamma + \theta) \mathbf{k}, \quad \omega_b = \dot{\theta} \mathbf{i}, \\ \mathbf{V}_b &= R\dot{\theta} \mathbf{j}, \quad \omega_c = (\dot{\gamma} + \dot{\theta}) \mathbf{i}, \\ \mathbf{V}_c &= (R\dot{\theta} - r(\dot{\gamma} + \dot{\theta}) \cos(\gamma + \theta)) \mathbf{j} \\ &\quad + (r(\dot{\gamma} + \dot{\theta}) \sin(\gamma + \theta)) \mathbf{k}, \end{aligned} \quad (1)$$

where γ , θ , r , R , \mathbf{D}_{co} are respectively the rotation angles of core and sphere, the distance of the core from the center of the circular pipe, the radius of the spherical body, the position of the rotating mass-point (core). We can now introduce the Lagrange-Euler function $E_L = E_k - E_p$ that contains only the terms due to the rotation along the $O - Y$ axis, where E_k and E_p stand for the total kinetic and potential energies. By considering the spherical shell as a rigid body and the core as a mass-point, E_L is

$$E_L = \frac{1}{2}M_b|\mathbf{V}_b|^2 + \frac{1}{2}I_b|\omega_b|^2 + \frac{1}{2}m_c|\mathbf{V}_c|^2 + m'_c g d_c, \quad (2)$$

where M_b , m_c , m'_c , $I_b = 2M_bR^2/3$, g and d_c are the mass of whole body except the core, the mass of the core, the core's apparent mass due to existing body forces, the inertia tensor of rolling body, the acceleration of gravity and the distance of the core respect to the ground, respectively. Note that the apparent mass of the core m' is due to the gravity and buoyancy forces¹. After the substitution of Eq. (1) into

¹Please refer to Eq. (22) for the derivation.

(2), we will get

$$\begin{aligned} E_L &= \frac{1}{2}R^2\dot{\theta}^2M_b + \frac{1}{2}I_b\dot{\theta}^2 + m'_c gr(1 - \cos(\gamma + \theta)) \\ &\quad + \frac{1}{2}m_c \left[(R\dot{\theta} - r(\dot{\gamma} + \dot{\theta}) \cos(\gamma + \theta))^2 \right. \\ &\quad \left. + (r(\dot{\gamma} + \dot{\theta}) \sin(\gamma + \theta))^2 \right]. \end{aligned} \quad (3)$$

Now, the Lagrange-Euler equations for translation in $O - Y$ plane is as follows:

$$\frac{d}{dt} \left(\frac{\partial E_L}{\partial \dot{\gamma}} \right) - \frac{\partial E_L}{\partial \gamma} = \tau_\gamma, \quad \frac{d}{dt} \left(\frac{\partial E_L}{\partial \dot{\theta}} \right) - \frac{\partial E_L}{\partial \theta} = \tau_\theta, \quad (4)$$

where τ_γ and τ_θ are the external torques for the core and the sphere. As we assumed the core as a mass-point, it doesn't contain any spinning around itself hence reactive torque between core-body is $\tau_\theta = 0$. Therefore, equations of the motion for the given mechanical system from Eq. (3)-(4) can be represented in following form

$$\begin{bmatrix} M_{11} & M_{12} \\ M_{21} & M_{22} \end{bmatrix} \begin{bmatrix} \ddot{\theta} \\ \ddot{\gamma} \end{bmatrix} + \begin{bmatrix} N_{11} \\ N_{21} \end{bmatrix} + \begin{bmatrix} G_{11} \\ G_{21} \end{bmatrix} = \begin{bmatrix} \tau_\gamma \\ 0 \end{bmatrix}, \quad (5)$$

where M_{ij} , N_{ij} and G_{ij} are the acceleration coefficients, the velocity dependencies and the gravity factors, while:

$$\begin{aligned} M_{11} &= M_{12} - m_c R r \cos(\gamma + \theta) = m_c r^2 \\ &\quad - m_c R r \cos(\gamma + \theta), \\ M_{21} &= M_{22} + M_b R^2 + I_b + m_c R^2 - m_c R r \cos(\gamma + \theta) \\ &= M_b R^2 + I_b + m_c R^2 - 2m_c R r \cos(\gamma + \theta) + m_c r^2, \\ N_{11} &= 0, \quad N_{21} = m_c R r (\dot{\gamma} + \dot{\theta})^2 \sin(\gamma + \theta), \\ G_{11} &= G_{21} = m'_c r g \sin(\gamma + \theta). \end{aligned} \quad (6)$$

III. MODEL OF DRIVING MECHANISM

A. Fluid Actuator

To move the spherical mass (core) in the pipe, fluid flow is created by a linear actuator connected to the cylinder [see Fig. 2]. The core is manipulated with the created fluid displacement and control valves. Fig. 3 illustrates the schematic for the designed fluid actuator. We first model the connecting rod between the cylinder and linear actuator.

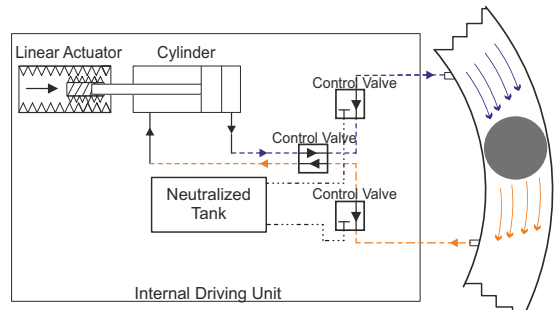


Fig. 2: Fluid actuated mechanism with flow control integration.

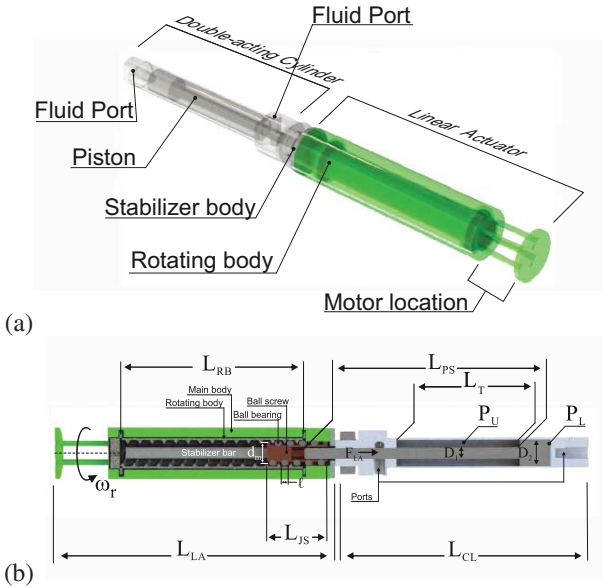


Fig. 3: Fluid actuator with a linear actuator and cylinder connection. DC motor torque is carried through rotating body to joint that is connected to cylinder rod.

Axial forces acting on the moving rod of the cylinder and linear actuator are defined as follows

$$F_I - F_L + F_S = 0, \quad (7)$$

where F_I , F_L and F_S are the inertia of cylinder's rod, the transferred joint force and the total friction force between the screw and rotating body, respectively. These forces are expressed by following equations [21]

$$F_I = m_L a_L, \quad F_L = 2\pi T_m \eta / \ell, \quad F_S = \mu_L F_I,$$

where m_L , a_L , T_m , η , ℓ and μ_L are the mass of rod and moving joint, the rod acceleration, the motor torque input, the efficiency of linear actuator, the lead size and the friction coefficient between rotating body and rod. Note that the efficiency for the involved lead in rotating actuator and ball screw is $\eta = [(\cos \alpha - \mu_s \tan \lambda) / (\cos \alpha + \mu_s \cot \lambda)]$ [21], where α , μ_s and λ are the thread angle, coefficient of friction (typically 0.15) in the screw and the lead angle. The screw is considered to be ball screw with minimal friction effect so η is approximated with 96%.

From the given parametrization, the motion equation of rod (7) can be represented as

$$\begin{aligned} \dot{D}_L &= V_L, \\ \dot{V}_L &= \frac{2\pi\eta}{m_L \ell (1 + \mu_L)} T_m, \end{aligned} \quad (8)$$

where the states are displacement and velocity of the rod. Since the connecting rod produces an equal displacement of the cylinder cl and the linear actuator L , we can assume $V_L = V_{cl}$. This property is later used on determining the fluid velocity in the pipes.

We are using the double-act cylinder. The volume in this cylinder tank is shifting in each cycle to provide a continuous flow during the simulation of Eq. (8). Thus, each side of the

tank produces the fluid with different pressure and velocity [see Fig. 3] where the affected cross-section area A_{cl} is

$$A_{cl} = \begin{cases} \pi D_2^2 / 4, & D_L \text{ is from } 0 \text{ to } L_T \\ \pi (D_2^2 - D_1^2) / 4, & D_L \text{ is from } L_T \text{ to } 0 \end{cases} \quad (9)$$

where D_1 , D_2 and L_T are the diameter of the rod, the diameter of the pusher in the cylinder and the length of the rod, in the given order.

B. Circular Pipe

The main part of the actuation mechanism, from the cylinder to the circulating core, operates in a liquid. In this system, a lightweight double-act pneumatic cylinder [22] is utilized as a pump actuator to create a continuous flow. The fluid is circulating inside a closed system so fluid volume is constant. Also, the flow moves through pipes, cylinder and neutralized tank. This liquid enters the neutralized tank to control the cylinder which fills the cycles inside the internal driving unit (IDU).

The fluid input ports and forces acting on the moving core are shown in Fig. 1-b. We construct the motion equation where the core and fluid are interfacing. It is assumed that flow velocity in the pipe is the same as the velocity of the core $\mathbf{V}_c = r\dot{\gamma}\mathbf{n}$, where $\dot{\gamma}$ and \mathbf{n} are the core angular velocity and the unit vector tangent to the circular path of the pipe. The proposed mechanism works in the liquid-solid medium; hence we combine the given core forces with the fluid input by using the flow momentum equation [23], [24] as follows

$$\frac{d(m_c \mathbf{V}_c)}{dt} = \oint\!\oint P_p \mathbf{n} dA_c + \iiint \rho_f \mathbf{g} d\nu_c + \mathbf{F}_v, \quad (10)$$

where P_p , dA_c , ρ_f , $d\nu_c$, \mathbf{g} and \mathbf{F}_v are the entering pressure to main pipe, the derivative of the core's cross-section area, the fluid density, the derivative of the core's volume, the gravity vector and the viscous forces on the moving core, in the given order. Also, $C.S.$ stands for the contour surface of the affected area by P_p . We model the system in polar coordinates where the left side of inertia has angular $\mathbf{a}_\gamma(t)$ and radial $\mathbf{a}_R(t)$ accelerations

$$\mathbf{a}_\gamma(t) = \frac{d|\mathbf{V}_c|}{dt} \mathbf{n} = r \frac{d}{dt}(\dot{\gamma}) \mathbf{n}, \quad \mathbf{a}_R(t) = -r\dot{\gamma}^2 \mathbf{m},$$

where \mathbf{m} is the unit vector in a radial direction. Please note that $\mathbf{a}_R(t)$ is ignored since it is constant with no effect on the core and the fluid; hence, all terms are expressed with respect to $\mathbf{a}_\gamma(t)$. Fluid pressure force as the first term in Eq. (10) can be obtained as

$$\mathbf{F}_P = \oint\!\oint P_p \mathbf{n} dA_c = P_p A_c \mathbf{n}, \quad (11)$$

where $A_c = \pi(R - r)^2$ is the constant cross-section area of the core. Next, the gravity term in Eq. (10) is decomposed to the core's gravity F_W and buoyancy F_B forces in which it is defined in tangent to the core path \mathbf{n}

$$\iiint \rho g d\nu_c \triangleq \mathbf{F}_W + \mathbf{F}_B = [-m_c + \rho_f \nu_c] g (1 - \cos \gamma) \mathbf{n}, \quad (12)$$

where $\nu_c = 4\pi(R - r)^3/3$ is the filled liquid volume of the core in the pipe. Also, \mathbf{F}_v consists of fluid head loss F_f and drag force F_D acting on the core's circular path [24]

$$\mathbf{F}_v = [F_f + F_D]\mathbf{n} = - \left(f_p \frac{L'_P}{D_c} \frac{V_c^2}{2g} + \frac{1}{2} C_D \rho_f A_c V_c^2 \right) \mathbf{n}, \quad (13)$$

where L'_P , D_c and C_D are the apparent length of the pipe, the diameter of the core and the drag coefficient, respectively. To keep the sign of the core velocity align with the rotation direction, the V_c^2 term in Eq.(13) is defined as $V_c^2 = r^2 \operatorname{sgn}(\dot{\gamma}_i) \dot{\gamma}^2$ where sgn is the sign function. Note that the head loss is a resistant force coming from bending form of the pipe. This force creates a centripetal acceleration due to secondary flow in the bend [24]. Thus, apparent length through the main pipe is

$$L'_P = L_P + [(K_b D_c)/f_p], \quad (14)$$

where L_P , K_b and f_p are the length of the circular pipe, the resistance coefficient for 180° in return bend and the Darcy friction factor in the entrance of the main pipe, respectively. From the definitions in Eqs. (11)-(13), Eq. (10) is transformed to the motion equation of the core as follows

$$F_P - F_W + F_B - F_f - F_D = m_c a_c, \quad (15)$$

where $a_c = r\ddot{\gamma}$ is the core tangential acceleration. The motion equation is formed with the assumption that the flux of linear momentum equilibrates with external forces, including pressure, gravity and the viscous friction forces. Please note that the flow continuum is definite since the surface gap between the pipe and the core is small.

Finally, to define the input pressure force P_p in Eq. (11), the two-stage Bernoulli equation with head loss is introduced within the streamline [23]:

$$\begin{aligned} P_{il} &= P_{cl} + \frac{\rho_f}{2} [V_{cl}^2 - V_{il}^2] - \rho_f g h_{il}, \\ P_p &= P_{il} + \frac{\rho_f}{2} [V_{il}^2 - V_p^2] + \rho_f g [Z_{il} - Z_p (1 - \cos \gamma_{il}) \\ &\quad - h_p], \end{aligned} \quad (16)$$

where P_{il} , V_{il} , P_{cl} , V_{cl} , V_p , h_p , Z_{il} , Z_p and γ_{il} are respectively the pressure and velocity of the fluid in the injection line, the pressure and velocity of the fluid in the cylinder, the velocity of entering fluid to the main pipe, the head-loss for transition of the cylinder to the injection line, the head-loss for transition of the injection line to the main pipe, the distance of injection line and the main pipe output ports from the ground and the angle of the injection line's port [see Fig. 1-b].

In the first stage, the fluid goes through the cylinder tank (P_{cl} , V_{cl}) to the injection line (P_{il} , V_{il}) where il stands for the slim fluid carrier pipe. The distance between the cylinder and injection lines is small ($h_{il} = 0$) as they both are in the box. To find out injection line pressure P_{il} , rod equations (8) are solved for V_{cl} . Next, the injection line velocity V_{il} is derived from continuity equation $V_{il} = V_{cl} A_{cl}/A_{il}$, where A_{cl} and A_{il} are the cross-section areas of the cylinder tank (9) and the injection line pipe. Then, cylinder pressure P_{cl}

TABLE I: Parameters of the driving mechanism.

Variable	Value	Variable	Value
$K_{S.E.}$	0.9	D_2	0.0097 m
K_b	0.2	d_m	0.0097 m
ℓ	0.007 m	D_{il}	0.00635 m
μ_L	0.75	D_c	0.028 m
m_L	0.2 kg	D_1	0.0047 m
η	96%	ρ_f	1000 kg/m ³
L_{IL}	0.145 m	γ_{il}	10°
L_T	0.05 m	T_m	0.27 mN · m
L_P	0.411 m	μ_f	1.81×10^{-3} kg/m · s
L_{JS}	0.01 m	I_b	0.0140 kg·m ²
C_D	0.8	g	9.8 m/s ²
M_b	1 kg	R	0.145 m
m_c	0.25 kg	r	0.131 m

$[2\pi T_m \eta]/\ell A_{cl}$ is substituted into (16) for establishing the injection line pressure P_{il} .

The injection lines (connecting both ports in Fig. 1) from IDU are connected to the main pipes with core (P_p , V_p). By the continuity equation $V_p = V_{il} A_{il}/A_c$, the velocity in the main pipe can be determined. Also, the head loss during the entrance of liquid to pipe from the injection line is defined as [23]

$$h_p = h_f + h_m = \frac{V_{il}^2}{2g} \left(f_{il} \frac{L_{IL}}{D_{il}} + K_{S.E.} \right), \quad (17)$$

where L_{IL} , h_f , h_m , D_{il} and $K_{S.E.}$ are the length of injection line pipe, the head loss of friction, the sudden expansion loss, the pipe diameter of the injection line and the loss coefficient through the transition from injection to the pipe, in the given order. These computations give P_p in (16). The cylinder tank and the pipe are assumed to be smooth surfaces; hence the friction factors for each section are calculated by

$$f_p = 64/Re_p, \quad f_{il} = 0.316/Re_{il}^{0.25},$$

where Re is the Reynolds number. Each of streamlines has its own Reynolds number as $Re = LV\rho_f/\mu_f$ where μ_f is the viscosity of rotating fluid. For instance, the Reynold number for pipe with the core p is $Re_p = L_P V_p \rho_f / \mu_f$.

IV. COMBINED MODEL OF ROLLING PIPE AND IDU

To combine the rolling body dynamics (5) with the driving mechanism (15), the input force of the core F_c has to be determined. Before calculating the core's input force, the created forces from fluid circulation are analyzed for elimination. From Eq. (15), the input force F_c can be written down as

$$F_c(t) = F_P - F_W + F_B - F_f - F_D - m_c a_c. \quad (18)$$

Lemma Let the external torque $\tau_\gamma = -rF_c$ of the core with distance r from the center of the sphere be on the right-hand side of motion equation of the rolling body (5). The introduced buoyancy, gravity and inertia forces in the IDU model have to be eliminated from (18) for establishing the combined model.

Proof: Consider (5)-(6) while this carrier body is steady ($\theta, \dot{\theta}, \ddot{\theta} = 0$), the core motion equation becomes:

$$\ddot{\gamma} [m_c r^2] + m'_c r g \sin \gamma = \tau_\gamma. \quad (19)$$

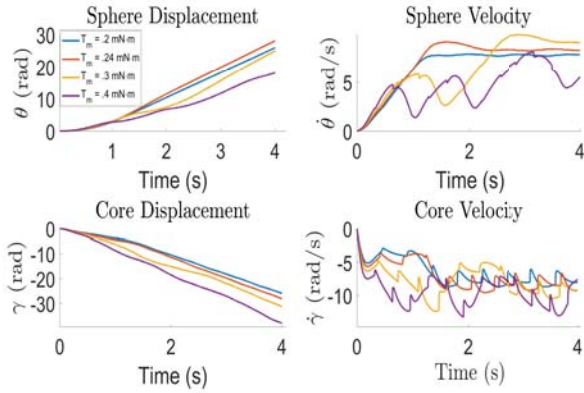


Fig. 4: First case analysis of obtained model with rest states.

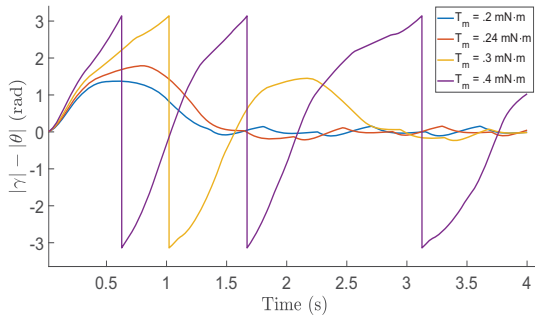


Fig. 5: The core location in sphere with respect to base frame for first case where $|\gamma| - |\theta| \in [-\pi, \pi]$.

Now, F_c in Eq. (18) is substituted into (19) as follows

$$\ddot{\gamma} [r^2 m_c] + r m'_c g_c \sin \gamma = r(-F_P + F_W - F_B + F_f + F_D + m_c a_c) \quad (20)$$

We can confirm that $F_W + F_B = m'_c g \sin \gamma$ and $a_c = r \ddot{\gamma}$. Thus, the body forces and the inertia terms of the core already exist in left-hand side of rolling body dynamics; hence, F_W , F_B and $m_c a_c$ have to be zero in Eq. (18). ■

Remark It can be interpreted that the head loss F_f , the drag F_D and the pressure F_P forces have to be included as external forces to the F_c .

By using the Remark, we can define the external torque with Eq. (11) and Eq. (13) as

$$\tau_\gamma = r F_c = r(F_P + F_f + F_D) = r \left[P_p A_c - 0.5 r^2 \operatorname{sgn}(\dot{\gamma}) \left(f_P \frac{L'_P}{D_c g} + C_D \rho_f A_c \right) \dot{\gamma}^2 \right] \quad (21)$$

Also, gravity and buoyancy forces at Eq. (12) are taken into account by using the apparent mass

$$m' = m_c - \rho_f \nu_c. \quad (22)$$

Thus, we substitute Eq. (21) and Eq. (22) to the motion equation of the rolling body in Eqs. (5), which results in the overall model of the system.

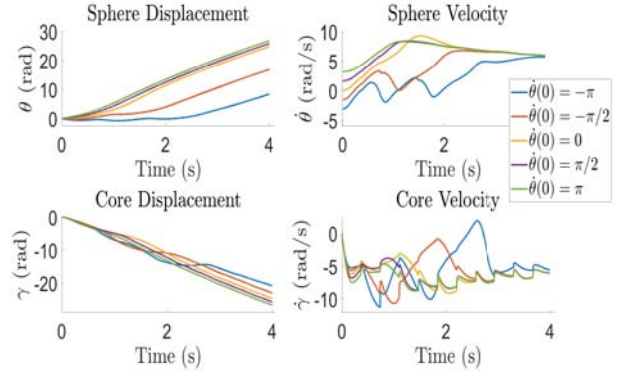


Fig. 6: The results of locomotion while carrier contains initial velocity $\dot{\theta}(0)$ as a second case.

V. MOTION SIMULATION ANALYSIS

We study the motion of the core in the circular pipe, propelling the carrier body. The total mass M_b is set as 1 kg with the core mass as 0.25 kg. The simulation lasts for 4 sec. Parameters of the driving mechanism are taken from Table I. The fluid actuator has the commercially available A07020D pneumatic cylinder [22] and DC motor 08GS61 [25]. Note that the chosen pneumatic cylinder can be used for moving the fluid and has a lightweight as 0.05 kg. To solve the complete model including Eqs. (5)-(6) and Eq. (8), ODE45 solver [26] in Matlab is chosen. The fluid pressure and velocities are calculated from Bernoulli equations in Eq. (16). The simulation analysis takes place for two cases: first, the combined model is checked for the ability to move the carrier when the core moves from the bottom of the pipe at rest states. Second, the carrier has different initial velocities with the same core location.

In the first case, the feed-forward control input is constant values for T_m . Fig. 4 illustrates simulation results of rolling body for various input torque values. We see that the sphere rolls in the given main direction (clockwise rotation) by the core's counterclockwise rotation. This confirms that the designed actuator successfully propels the carrier. However, there are minor fluctuations in core's velocity because as the cylinder stops to switch the cycles, it directly affects the system. This issue can be removed by using multiple cylinders to fill the gap of the filling cycles. Next, to demonstrate the core location with respect to the base frame, $|\gamma| - |\theta|$ is shown in Fig. 5. It is defined that $|\gamma| - |\theta| \in [-\pi, \pi]$. We see that two motion patterns appear in the system analysis. For a critical torque value $T_m = 0.24 \text{ mN}\cdot\text{m}$, the core stays in the lower hemisphere, which looks like the pendulum-actuated models. When the torque input is lower than these values, the core can't overcome viscous and gravity forces as the sphere turns. By exceeding the critical torque, the core starts circulating in the total pipe which creates a new pattern during locomotion.

It is observed that the resultant displacement of spherical carrier converges to lower values as the torque rises [see Fig. 4]. This demonstrates that higher control input doesn't always result in larger displacement. It is also clear that the core velocity shows large impulses with higher DC motor torque ($T_m \in [0.3, 0.4] \text{ mN}\cdot\text{m}$). Furthermore, high torque

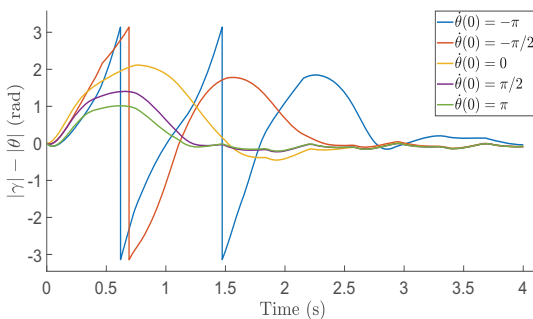


Fig. 7: Core location in sphere with respect to base frame for second case where $|\gamma| - |\theta| \in [-\pi, \pi]$.

input effects the clockwise rotation of the spherical carrier and creates minor backward locomotion (see Fig. 4 for θ angular displacement). For instance, when the core passes the north pole at approx. 0.6 sec with $T_m = 0.4$ mN·m [see Fig. 5], the sphere minor backward motion is observed in 1.5 sec (core arrives to bottom of sphere) in Fig. 4.

In the second case, the initial velocity of the carrier is not zero, $\dot{\theta}(0) \neq 0$. The control input is set as $T_m = 0.3e^{-t/T}$ mN·m where $T = 4$. The sphere initial velocity is limited to $\dot{\theta}(0) \in [-\pi, \pi]$.

It is obvious that the core is able to carry the sphere in the given main direction [see Fig. 6]. However, this spherical carrier reaches shorter distances as the initial velocity $\dot{\theta}(0)$ changes from π to $-\pi$. Also, the positive values of the sphere's initial velocities keep the core in lower-hemisphere [see Fig. 7], when the sphere orientation θ reaches the maximal distance. Also, the negative sphere velocities boost the actuated core to the north pole of the sphere [see Fig. 7]. This ability can have a negative effect on the final displacement of the carrier. As the core has this circulation around the pipe, the carrier travels less distance compared to the one established in the first case. Thus, the carrier can easily accelerate, but we have to control the core more accurately.

VI. CONCLUSION

A new fluid actuated driving mechanism for rolling bodies has been proposed and analytically studied in this paper. First, the dynamics of the rolling body on the plane were derived. Then, the described driving mechanism was modeled and combined with the rolling body model of the carrier. Simulation results show that the developed mechanism can successfully move the body with a feed-forward control. Moreover, the core rotation creates two motion patterns: swinging and circulation. As the core swings, the rolling body's behavior becomes similar to the conventional pendulum-actuated system. In the circulation pattern, the carrier body creates a different motion with a less arrival distance in contrast to swinging pattern. In future work, we will validate the obtained model with an experiment.

REFERENCES

- [1] Z. Li and J. Canny, "Motion of two rigid bodies with rolling constraint," *IEEE Trans. Robot. Autom.*, vol. 6, no. 1, pp. 62–72, Feb 1990.
- [2] R. H. Armour and J. F. Vincent, "Rolling in nature and robotics: A review," *J. of Bionic Eng.*, vol. 3, no. 4, pp. 195 – 208, 2006.
- [3] A. Halme, T. Schonberg, and Y. Wang, "Motion control of a spherical mobile robot," in *Proc. 4th Int. Workshop Adv. Motion Control (AMC 1996)*, vol. 1, Mar 1996, pp. 259–264.
- [4] A. Bicchi, A. Balluchi, D. Prattichizzo, and A. Gorelli, "Introducing the "SPHERICLE": an experimental testbed for research and teaching in nonholonomy," in *Proc. IEEE Conf. Robot. Autom.*, vol. 3, Apr 1997, pp. 2620–2625.
- [5] C. Wei-Hsi, C. Ching-Pei, Y. Wei-Shun, L. Chang-Hao, and L. Pei-Chun, "Design and implementation of an omnidirectional spherical robot omnicon," in *IEEE/ASME Int. Conf. Adv. Intell. Mechatron. (AIM)*, July 2012, pp. 719–724.
- [6] A. Chowdhury, G. S. Soh, S. Foong, and K. L. Wood, "Implementation of caterpillar inspired rolling gait and nonlinear control strategy in a spherical robot," *J. of Bionic Eng.*, vol. 15, no. 2, pp. 313–328, 2018.
- [7] A. H. J. A and P. Mojabi, "Introducing august: a novel strategy for an omnidirectional spherical rolling robot," in *Proc. IEEE Int. Conf. on Robot. and Autom.*, vol. 4, 2002, pp. 3527–3533.
- [8] A. Behar, J. Matthews, F. Carsey, and J. Jones, "NASA/JPL tumbleweed polar rover," in *Proc. IEEE Aerospace Conf.*, vol. 1, March 2004, p. 395.
- [9] D. Liu, H. Sun, and Q. Jia, "Stabilization and path following of a spherical robot," in *Proc. IEEE Conf. Robot. Autom. and Mechatron.*, Sept 2008, pp. 676–682.
- [10] S. Mahboubi, M. Seyyed Fakhreabadi, and A. Ghanbari, "Design and implementation of a novel spherical mobile robot," *J. Intell. Robot. Sys.*, vol. 71, no. 1, pp. 43–64, 2012.
- [11] R. Mukherjee, M. A. Minor, and J. T. Pukrushpan, "Motion planning for a spherical mobile robot: Revisiting the classical ball-plate problem," *Journal of Dynamic Systems, Measurement, and Control*, vol. 124, no. 4, pp. 502–511, 2002.
- [12] E. Kayacan, E. Kayacan, H. Ramon, and W. Saeys, "Adaptive neuro-fuzzy control of a spherical rolling robot using sliding-mode-control-theory-based online learning algorithm," *IEEE Trans. Cybern.*, vol. 43, no. 1, pp. 170–179, 2013.
- [13] F. R. Hogan and J. R. Forbes, "Trajectory tracking, estimation, and control of a pendulum-driven spherical robot," *J. Guid. Control Dyn.*, pp. 1119–1125, 2015.
- [14] J. Brown, H.B. and Y. Xu, "A single-wheel, gyroscopically stabilized robot," in *Proc. IEEE Int. Conf. on Robot. and Autom.*, vol. 4, Apr 1996, pp. 3658–3663.
- [15] S. Bhattacharya and S. Agrawal, "Spherical rolling robot: a design and motion planning studies," *IEEE Trans. Robot. Autom.*, vol. 16, no. 6, pp. 835–839, 2000.
- [16] A. Morinaga, M. Svinin, and M. Yamamoto, "A motion planning strategy for a spherical rolling robot driven by two internal rotors," *IEEE Trans. Robot.*, vol. 30, no. 4, pp. 993–1002, 2014.
- [17] G. C. Schroll, "Design of a spherical vehicle with flywheel momentum storage for high torque capabilities," Master's thesis, Massachusetts Institute of Technology, Cambridge, MA, 2008.
- [18] S.-S. Ahn and Y.-J. Lee, "Novel spherical robot with hybrid pendulum driving mechanism," *Advances in Mechanical Engineering*, vol. 6, p. 456727, 2014.
- [19] A. Koshiyama and K. Yamafuji, "Design and control of an all-direction steering type mobile robot," *Int. J. Robot. Res.*, vol. 12, no. 5, pp. 411–419, 1993.
- [20] S. A. Tafrishi, "'RollRoller' novel spherical mobile robot basic dynamical analysis and motion simulations," Master's thesis, University of Sheffield, Sheffield, UK, 2014, available at <http://arxiv.org/abs/1610.06043>.
- [21] P. R. Childs, *Mechanical Design*, 2nd ed. Butterworth-Heinemann, 2003.
- [22] AutomationDirect. (2018) "A-series double-act pneumatic cylinders". Accessed November 19, 2018, www.automationdirect.com.
- [23] R. L. Street, G. Z. Watters, and J. K. Vennard, *Elementary Fluid Mechanics*, 7th ed. New York, USA: Wiley & sons, 1996.
- [24] D. F. Young, B. R. Munson, T. H. Okiishi, and W. W. Huebsch, *Brief Fluid: A Brief Introduction*, 5th ed. USA: Wiley & sons, 2010.
- [25] Trident Engineering. (2018) "GS61-series DC motor". Accessed November 19, 2018, www.tridenteng.co.uk.
- [26] J. Dormand and P. Prince, "A family of embedded Runge-Kutta formulae," *J. Comput. Appl. Math.*, vol. 6, no. 1, pp. 19–26, 1980.